Oscilloscopic Capture of Greater-than-100 GHz, Ultra-low Power Optical Waveforms Enabled by Integrated Electro-Optic Devices

Xiaoxi Wang, Boris A. Korzh, Peter O. Weigel, Deacon J. Nemchick, Brian J. Drouin, Wolfgang Becker, Qing-Yuan Zhao, Di Zhu, Marco Colangelo, Andrew E. Dane, Karl K. Berggren, Matthew D. Shaw, and Shayan Mookherjea

Abstract—Direct time-domain sampling oscilloscopic capture of ultra-high bandwidth (32-102 GHz) modulated optical waveforms at 1550nm is demonstrated at optical power levels below -100dBm. To detect fast optical waveforms directly at power levels far below what traditional optical oscilloscope methods can measure, we use a time-correlated single-photon counting (TCSPC) sampling acquisition method, recently-developed integrated electro-optic devices with >100 GHz electro-optic bandwidth and single photon detectors with < 5 ps jitter. We show the reconstruction of the time domain signals by collecting histograms of time-binned single photons captured using TCSPC, and characterize the spectral components in the frequency domain. The ability to acquire ultraweak eye diagrams and identify high-frequency spectral components from a relatively small ensemble of single-photon measurements may lead to significant advances in optical waveform capture technology.

Index Terms—Ultrafast measurements, Photon counting, electro-optic modulators, single-photon detectors, optical receivers, oscilloscopes.

I. INTRODUCTION

CAPTURING fast (>100 GHz modulation bandwidth) optical signals in the femtowatt power regime (-100 dBm, approximately) directly in the time domain is fundamentally challenging due to the proportional scaling of detectivity with bandwidth. The minimum power of a signal that can be acquired by a state-of-the-art 110 GHz analog bandwidth oscilloscope is about -48 dBm after extensive averaging is performed [1],[2]. For capturing modulated optical signals, the photodiodes which support 100 GHz modulation bandwidth require milliwatt power levels [3], and since electrical power generated by a linear photodiode bears a quadratic relationship to optical power, there is a steep roll-off in performance with

decreasing average optical powers. Avalanche photodiodes can have a high gain-bandwidth product, but do not scale to such high bandwidths. Further improvements in optical oscilloscope technology, even with the aid of sophistical electronic signal processing, are expected to be extremely challenging [4],[5].

Here, we show a different approach to capturing modulated optical waveforms capable of scaling to very low power levels, down to a single photon detection event per cycle of a measurement clock, which is typically 80 MHz range in our experiment, but could be faster or slower depending on the input power level and the detector characteristics, as described below. We use recently-developed electro-optic modulators, superconducting nanowire single photon detectors (SNSPDs) and time-correlated single photon counting (TCSPC) electronics, to perform time-domain waveform capture of optical signals at a wavelength of 1550 nm in the femtowatt (approximately 64 fW) average power regime and analog bandwidths exceeding 100 GHz. Generally, TCSPC techniques [6], [7], due to their simplicity, reasonable cost, and calibrationfree nature, are often used in spectroscopy, ranging, and imaging [8]-[10]. Over the past decade, oscilloscopic measurement of signals with up to about 1-10 GHz effective measurement bandwidth has been achieved using available components [11]-[13], which is substantially improved upon here by using newly designed and fabricated electro-optic components (Mach-Zehnder modulators [14] and SNSPDs [15]). The method shown here achieves both extremely high bandwidth and extremely low sensitivity. Several other highbandwidth optical waveform capture methods have been studied, based on optical mixing, amplification, sampling, dispersive, and nonlinear techniques, and some are capable of single-shot, rather than sampling, acquisition, but they all require at least tens or hundreds of microwatts of signal power

This work was supported in part by National Science Foundation (ECCS 1201308, EFMA-1640968), NASA (NNX16AD14G, 80NSSC17K0166), and the DARPA Defense Sciences Office, through the DETECT program.

X. Wang and P. O. Weigel are with the Department of Electrical and Computer Engineering, University of California, San Diego 92093 (e-mail: xiw270@ucsd.edu).

B. Korzh, D. J. Nemchick, Brian J. Drouin and M. D. Shaw are with the Jet Propulsion Laboratory, California Institute of Technology, 4800 Oak Grove Drive, Pasadena, California 91109, USA.

Q.-Y. Zhao, D. Zhu, M. Colangelo, A. E. Dane and K. K. Berggren are with the Department of Electrical Engineering and Computer Science, Massachusetts Institute of Technology, Cambridge, Massachusetts 02139, USA.

W. Becker is with Becker & Hickl GmbH. Nahmitzer Damm 30, D-12277 Berlin, Germany

S. Mookherjea is with the Department of Electrical and Computer Engineering, University of California, San Diego 92093 (e-mail: smookherjea@ucsd.edu).

[16]-[23], about nine orders of magnitude more than required here.

II. HIGH SPEED WAVEFORM SAMPLING BY PHOTON COUNTING

The instrumentation described here is shown schematically in Fig. 1. Light from a continuous-wave diode laser at 1550 nm was modulated using an electro-optic modulator driven by high-frequency RF signals, which could be either sinusoidal waves or data waveforms depending on the application and available test equipment. The modulated lightwave signal was attenuated down to an average power level around -100 dBm and was detected using a single-pixel superconducting nanowire single-photon detector (SNSPD). Each photon detected by the SNSPD generated a "start" pulse for a TCSPC card. A periodic electrical clock (here, at 80 MHz) was sent to one of the electrical inputs of the TCSPC card and generated the trigger of the "stop" signal. The clock is phase stabilized with respect to the modulation test pattern, as with all sampling oscilloscopes. The clock frequency should be chosen so that there is no more than one detection event in each clock cycle. Thus, a faster clock cycle is required for handling higher input powers by this technique, while keeping in mind that singlephoton detectors have a reset time after each detection event. On the other hand, it is not a problem to have many time bins with no detection events; these do not contribute to the digital data bandwidth handled by the card. The start-stop time difference Δt_{Bin}, was acquired repeatedly (N1, N2, ... labels the time bins) and the resulting histogram gradually reproduced the input waveform. A total acquisition time of about 2 minutes was sufficient for the measurements reported here, and we study the improvement in the signal-to-noise ratio with acquisition time in Section VI. In these experiments, each photon detection event was also time-stamped, in order to characterize the buildup of the histogram over time; however, this is not required in routine operation.

III. FAIR SAMPLING OF THE INPUT WAVEFORM

Each event building up the start-stop histogram can be viewed as having been caused, under the correct operating conditions, by a randomly selected photon with uniform probability from the entire waveform. In the very low average power regime, the photons from the incoming waveform constitute a Poisson process at the detector, and the detection method randomly samples single detection events for histogramming. The experimental apparatus and operating conditions should ensure that the random sampling should be independently and identically distributed, since under such conditions, the random selection of a Poisson process is itself a Poisson process, the entire waveform will get "fair sampled" over time i.e., acquired without truncation, omission or bias towards either the head or tail of the message.

Fig. 2 reports on an experiment demonstrating the concept using standard, commercially available instruments: a conventional 10 Gbit/s lithium niobate electro-optic modulator (EOM, Optilab), tungsten silicide (WSi) SNSPD (Photon Spot

Inc.) and TCSPC card (TimeHarp 260, PicoQuant GmbH). The EOM was used to modulate the light at 1550 nm from an external-cavity tunable single-mode semiconductor laser (Keysight). A modest extinction ratio of about 7 dB was used, in order to model a typical digital optical communications data stream. (At a single bias current setting, the SNSPD can detect a dynamic range of at least 40 dB, given the ratio of the maximum count rate, which is a few megahertz, to the dark count rate, which was less than 100 Hz.) The data signal was generated from an ASCII code, in binary representation, of some English language text, by an arbitrary waveform generator (Keysight), under computer control. After suitable attenuation, the optical waveform was detected using a conventional sampling oscilloscope (DCA-X, Keysight) with a single-mode fiber coupled optical front-end module, which is shown in Fig. 2(a) and using the readout of a WSi SNSPDs operated in a cryostat at 0.8K (PhotonSpot Inc.) and acquired using a TCSPC card (TimeHarp 260, PicoQuant GmbH) used in a computer workstation, which is shown in Fig 2(b). Here the waveform was measured with a (relatively coarse) resolution of about 25 ps, in order to capture a long end-to-end measurement window. The fiber-coupled, free-running WSi SNSPD has a system detection efficiency, SDE > 90% (due to a resonant cavity design) for 1550 nm and the jitter was estimated to be about 70 ps. The TCSPC card performs, effectively, a 15-bit time-to-amplitude conversion, and has a dead time of 25 ns when used with a time bin resolution of 25 ps. The dead time (25 ns) is therefore substantially smaller than the time window that is captured. Fig. 2(c) compares the detection of a nonreturn-to-zero (NRZ) message using both a conventional sampling oscilloscope and the start-stop technique. The horizontal axis in Fig. 2(d) is the time window over which the mathematical cross correlation between the traces in Fig. 2(a) and 2(b) is calculated, and ranges from a small window (about 10% of the total span) to the entire recorded waveform. These measurements demonstrate that the individual bits as well as the entire bit pattern were captured with high fidelity. The cross correlation over both narrow and wide time bases shows that there is little bias or tilt in the fairly sampled waveform across the entire collected measurement. The average optical power at the detector input of the conventional sampling oscilloscope was -7 dBm (200 µW), whereas it was only -112 dBm (6.3 fW) for our scheme.

IV. EXPERIMENTAL DETAILS

To study the modulation traces of the highest RF frequencies that could be captured, the EOM device used in the results reported in Fig. 3 was a research-grade hybrid EOM device in the Mach-Zehnder configuration, in which unetched thin-film lithium niobate (LN) was oxide-bonded to silicon photonic waveguides [24]. The modulator uses hybrid modes which are mainly location in the LN region, with a small portion in the Si and SiO₂ regions. There was no lithography performed in the LN layer; all the waveguiding features were defined by lithography only in the Si layer. The hybrid waveguide was

formed as a Si rib loading the LN slab, with a thin oxide gap for appropriate selection of the best optical mode refractive index. The bonding was performed at room temperature, with a low temperature anneal step (200 °C). After handle removal, aluminum electrodes (thickness 1.8 µm) were deposited and patterned in a co-planar waveguide ground-signal-ground configuration. Tapers and bends were used in the microwave feeder section as described in [24]. To define the optical pathway of the Mach-Zehnder interferometer, the optical mode was coupled, split, and routed in silicon waveguide components (the cladding consisting only of SiO₂) outside the bonded region, and then made vertical transitions in to and out of a hybrid mode that is predominantly guided in the LN region by varying the rib-loading silicon waveguide width underneath the LN thin film. Precision silicon lithography, carried out at waferscale using a deep ultraviolet (DUV) foundry process at the Sandia National Laboratories, resulted in accurate definition of the layer thicknesses and waveguide width. This resulted in good optical-RF phase matching to very high frequencies, beyond 100 GHz. The modulators measured here have greater than 140 GHz 3-dB electrical modulation bandwidth inferred from direct modulation-sideband measurements up to 110 GHz (at which the 3-dB point is not yet reached), and a measured value of $V_{\pi}L = 6.5$ V.cm. Optical input and output coupling was achieved using lensed and tapered polarization-maintaining fibers, and multi-axis positioning stages.

The modulated optical signals were detected using a lowjitter niobium nitride SNSPD with cryogenic amplification of the detector signal [25]. The SNSPD detectors were specially designed in a microbridge structure (5 µm long) to minimize the geometric jitter and noise jitter that had previously dominated the jitter masking the inherent timing resolution performance of the detectors. The detectors operated with a saturated internal efficiency meaning that each photon absorbed in the metal nanowire lead to a detection signal. A customized, high-resolution, low-jitter TCSPC card was used (currently, the highest-reported photon timing resolution, 200 fs). The combination of the SNSPD, amplifier and (room temperature) TCSPC card was measured to have an instrument response function (IRF) of 6.3 ps full-width at half-maximum at 1550 nm as shown in Fig. 4. To acquire the eye diagrams shown in Fig. 3, a time-bin resolution of 200 fs was used at the TCPSC card. The combination of the IRF and the bandwidth limitations of the EOM and available test equipment define the highest frequency (slightly above 100 GHz) that we can presently capture at 1550 nm wavelengths. These modulation frequencies are far higher than the analog bandwidth of commercially available arbitrary waveform generators (approximately 45 GHz), and hence, the test modulation patterns in Fig. 4 were sinusoidal waves generated from millimeter-wave RF oscillators rather than binary digital data patterns as in Fig. 2.

The microwave signal was generated directly, for frequencies up to 40 GHz, from a swept-frequency microwave CW oscillator (Anritsu), with a Rubidium clock reference signal at 10 MHz. For generating RF frequencies from 32 GHz - 40 GHz, an RF amplifier (MITEQ) bandlimited to about 26 GHz - 40 GHz was used. For generation of RF frequencies

greater than 40 GHz, a multiplier chain was used, consisting of an RF synthesizer, 6x multiplier (Millitech) covering the frequency range 75 GHz – 110 GHz (approximately), along with GaAs and GaN amplifiers. The output of the amplifier chain was coupled to a WR-10 waveguide, which was adapted to a 1.0 mm RF cable (for reasons of compatibility with the test station). The RF swept-frequency source also provided a 10 MHz reference, which was used by an arbitrary waveform generator (Tektronix) to generate a steep-transition output trigger at 80 MHz. The mm-wave signal was incident on the modulator microchip using $50-\Omega$ GSG probes rated to 110 GHz. Calibration of the signal pathway was performed using a highfrequency RF power sensor and calibration substrates. The generated signal showed a 50% power drop from 102 GHz to 104.88 GHz and 98% power drop beyond 104.88 GHz; thus, the latter number (approximately 105 GHz) was the highest frequency used in this experiment.

The histogram was captured in the reverse start-stop mode. A free-running NbN SNSPD with negligible after-pulsing and low dark counts (<50 Hz) was used to generate the 'start' signals, whereas the 'stop' signal was generated by a conventional electronic clocking waveform, derived from a stable rubidium time source as described earlier. The SNSPD was cooled below 1K using a closed-cycle Helium-4 sorption refrigerator. Light was coupled onto the detector through freespace windows and filters, using a lens located outside the cryostat, yielding an efficiency of approximately 10⁻⁴. By placing the lens inside the cryostat is it possible to increase the single photon detection efficiency to the 1% level. Further improvements in efficiency are possible by utilizing a differential architecture of the detector, in order to increase the active area, by cancelling out the geometric jitter[26], as well as imbedding the device into an optical stack[27]. In addition to the IRF shown in Fig. 3, an additional, though minor, contribution to the system jitter was the jitter (1.5 ps) measured between the trigger signal and the RF signal driving the modulator. Critical to achieving high resolution is achieving a short and stable rise time (t_R) of the SNSPD signal, which is given by the ratio of the kinetic inductance (L_{k} ~ 80 nH) and the sum of the normal domain resistance $R_N \sim 1~k\Omega$ and load resistance $R_L \sim 50 \Omega$, thus achieving $t_R \sim 80$ ps. Low-noise RF amplifiers (Cosmic Microwave Technology) were used to readout the SNSPD signal and were placed on the 4 Kelvin stage of the cryostat. The bandwidth of the RF signal transmitted to the TCSPC card was about 3 GHz, which is adequate for the present purpose, and is not the limiting factor in determining the highest frequency modulation content (beyond 100 GHz [28]) that can be detected using the measurement technique reported here.

The output of the RF amplifiers was captured using a PCIe TCSPC module (SPC-150NXX, Becker and Hickl) in a computer workstation. By increasing the TAC transfer ratio (time-to-voltage ratio), a minimum time channel width of 204 fs was obtained, as well as reduced TAC readout noise. High-frequency cables and connectors were not required between the amplifier and the TCSPC board. The electronics converted the time interval between the detection event and the clock signal

to a voltage using a calibrated time-to-amplitude converter (TAC) circuit, and the voltage signal was read out by a high-resolution analog to digital converter (ADC). The ADC was not required to operate at the Nyquist bandwidth of the optical signal, since it is only the jitter in the interval between the start-stop events, corresponding to an imprecision in incrementing the appropriate histogram bin, which eventually imposes the effective bandwidth limitation. Increasing the trigger rates in reverse start-stop counting cards can mitigate pileup; here the trigger frequency was set to 80 MHz giving a 12.5 ns period ($T_{\rm Trigger} = 12.5$ ns). The TCSPC card used in Figs. 4, 5 and 6 required $T_{\rm dead} = 100$ ns dead time (regardless of the computer speed), which imposed a limit on the maximum count rate in these experiments. Future improvements in the dead time of the card would allow higher count rate detectors to be used.

V. SIGNAL EXTRACTION AND RECONSTRUCTION

In our proof of principle demonstrations, thermal drift of the devices was not stabilized and a slow phase drive in the optical waveform out of the modulator was observed as Fig. 5 shows. To correct for the phase drift in the high-speed experiments of Fig. 4, the raw measured time-tags of the photon detection events acquired over a typical experimental run of 120 seconds were assembled into 10 second blocks in increments of 0.1 seconds. Each segment was fitted with a sinusoid function whose mean value (i.e., the vertical shift) was a fitted parameter, in accord with the sinusoidal modulation imposed on the electro-optic modulator, using a nonlinear least-squares algorithm. The blocks were chosen to be large enough so that the standard error of the fit was smaller than the slope of the largest phase drift per unit time. The fitted phase-offset term is plotted over the (120 seconds) measurement time in Fig. 5, and was seen to vary slowly and by a relatively small amount, less than 0.19 radians root-mean-square of drift. Such slow phase drifts can be due to the lack of bias-point stabilization on the research-grade electro-optic modulator microchip, the noise picked up in the RF cables, or a slow rotation in the state of polarization of the laser light incident on the modulator, which was also not feedback-stabilized, or some combination of these effects. The traces shown in Fig. 4, and those that were processed for the generation of Fig. 6, have had this slow phase drift removed from the raw data by post-processing. The differences between the waveforms before and after phase drift correction are minor, as shown visually in Fig. 5(d), but the waveform with the phase drift removed leads to a more accurate calculation of Signal-to-Noise Ratio (SNR) between different measurements. In the current experimental setup,

Fig. 4(a) reports the calculation of a figure-of-merit, labeled SNR, defined as the ratio of the mean signal power over twice the standard deviation of the noise power. This SNR was calculated across the entire Nyquist bandwidth of the effective sampling frequency, determined by the duration (200 fs) of a single time bin. The noise signal was computed by the subtraction of the measured data points from a vertically shifted sinusoid fit to the data (nonlinear least-squares fitting procedure). The fit was performed after phase-drift removal and correcting for time-bin nonlinearity across the measurement epoch (4096 bins cumulatively addressing 0.8

ns). It was verified that a subtraction of the raw data from the line of best-fit did not result in any observable periodicity or identifiable skew in the residual trace, which was therefore, taken as a noise signal for purposes of calculating the SNR. The eye diagram reconstructions were performed by folding over successive segments of the processed waveform onto the same horizontal time base, and are shown in Fig 3(b)-(f). In this comparative SNR calculation, by successive segmentation in the time domain to correct for phase drift and time-bin nonlinearity, the deviation from the vertically shifted sinusoid fit or higher harmonics was not considered, and neither was the error margin; therefore, the SNR here is a lower bound. We note that the capture method in the current experimental setup is based on a repetitive trigger and is not a single-shot capture. While the current post processing is used to correct the drift of sinusoids, clock synchronization [29] and timebase correction methods can be used for non-sinusoidal signals [30], and multidetector based interferometric schemes for phase estimation

VI. FREQUENCY DOMAIN CHARACTERIZATION

Fig. 6 reports the SNR as a function of the number of detected photons, at various RF frequencies. In the frequency domain, SNR is defined differently than in the time-domain traces studied in Fig. 4. Here, the SNR is defined in terms of the power spectral density in the frequency domain (consistent with the definition of SNR usually used in the calculation of the effective number of bits, ENOB), and was calculated as the ratio of the signal power to the integrated noise power across the 200 picosecond sampling bandwidth. To calculate the power spectral density, a fast-Fourier-transform was performed on the entire measurement set of the full acquisition time of the phasedrift-corrected time-domain waveform of whose length was approximately 4096 time-bin samples (minus an appropriate number of time bins to make the data periodic prior to windowing). To estimate the power density spectrum as a Fourier-transform of the autocorrelation function, the accumulated photon counts are first converted to units of power on a linear scale (Watts) by accounting for the acquisition time. This approximates the mean power and a fast-Fourier-transform on the measurement set gives the power spectrum. The noise bandwidth was then taken to be the entire Nyquist-sampling range (i.e., the inverse of the temporal duration of the single bin width, 200 fs), minus a number of frequency bins around the signal equal to one-half of the signal bandwidth. The noise power was estimated by summing these noise bins across the noise bandwidth and weighting the average by a fourth-order central moment of the distribution of noise bins. For a Poisson distribution, the fourth-order central moment was taken as the mean plus three times the square of the mean. With the assumption that the noise floor is spectrally flat, the fourth order central moment was multiplied by a weight term and added to the variance such that the noise floor was taken to be four standard deviations away from the mean. Since the noise floor has a distribution about the average of the noise bins, this weights the upper tail of the noise floor more (decreases the estimated SNR). Finally, the peak value of the signal power spectral density was multiplied by the same number of noise bins as used in the noise bandwidth calculation, and was then divided by the noise power. This approximates the definition of Optical Signal-to-Noise ratio (OSNR) typically used in optical spectrum analyzers to estimate the ratio of peak signal power to the noise floor by taking the data points representing the noise floor a specific bandwidth away from the signal, as in a dense-wavelength-division-multiplexing communication channel.

The capture time, expressed as the number of photons needed to reach a target SNR, is studied in Fig. 6. As shown in Fig. 6(a), SNR improves in all cases with increased acquisition time. The maximum achievable dynamic range is ultimately limited to about 60 dB, based on the ratio of the maximum count rates achievable from the SNSPD detector (a few million counts per second) to the dark count rate (a few counts per second). The factors in the current experimental setup that limits the dynamic range in the raw data of photon counts are the capture time window of the TCSPC card when set to its highest resolution, and the long tail of the instrument response function, which must be deconvolved to back-calculate the true dynamic range. In the current experimental setup, the capture time window, also called "epoch", is $T_W = 2^{12}$ bins x 0.2 ps/bin = 0.8 ns. The ratio $T_{\text{Trigger}}/T_{\text{W}}$ thus defines the "filling factor", $\eta_{\text{valid-trigger}} = 15$. Thus, the number of photons that was registered and binned by the TCSPC card is lower than the actual number of photons "consumed" by the SNSPD detector, by a factor of $\eta_{valid-trigger}$. By adding parallel TCSPC cards and utilizing the full trigger speeds, the overall capture time can be readily improved, and capture of the entire (memory-limited) temporal epoch would be possible, similar to the measurement reported in Fig. 2.

Figure 6(b) shows the time needed to reach a threshold SNR that is acceptable for identification of the signal from its (Fourier) spectrum. For simplicity, we take the threshold to be SNR=5 dB. Fig. 6(b) shows that, at an incident photon rate of about 0.5 MHz, detection of photons over about 6 milliseconds is adequate at $f_{RF} = 40$ GHz, and the required acquisition time increases to about 150 milliseconds for $f_{RF} > 100$ GHz. Figs. 6(c)-(d) show representative examples of the power spectrum of the waveform, identifying the carrier frequency above the noise floor at capture times well short of 120 seconds.

VII. DISCUSSION

It should be noted that SNSPDs themselves, like many other single-photon detectors, require time for reset after each detection event; here, the SNSPD reset time was 10 ns but due to AC coupling of the cryogenic amplifier, at least 100 ns was required to avoid detector re-biasing. The average reset time was smaller than the average inter-arrival time of detected photons (approximately 1 us in Fig. 4, and 10 us in Fig. 2) in order to avoid pile-up [32]. Additionally, the combination of multiple detectors addressed through temporal segmentation, along with increased memory, may enable long continuous sequences of data to be acquired. Single-chip-based multichannel time-to-digital converter systems with adequately low jitter have been developed [33], which could reduce the cost of a multi-channel system and enable simpler synchronization in the future. The acquisition time can be decreased, and seamless coverage of the temporal window can be achieved by simply parallelizing the TCSPC electronics and using multiple

detectors. Although the SNSPD detector is cryogenically cooled, the cost and complexity of closed-cycle cryocoolers is rapidly dropping, and more than a dozen detectors can be housed in a single system. The method described here avoids the Nyquist requirement, i.e., does not require generation or propagation of a signal at twice f_{RF} (i.e., at 210 GHz) anywhere in the instrumentation. Nyquist-rate filtering or scan synchronization is very challenging at these millimeter-wave frequencies, and our method also does not require the RF cabling or connectors to support such a high bandwidth, which would be costly, and difficult to operate and calibrate.

VIII. CONCLUSION

In summary, we have demonstrated, for the first time, the eye-diagram capture of ultra-broadband (greater than 100 GHz bandwidth) modulated optical waveforms at a wavelength of 1550 nm at ultra-low (less than -100 dBm) average power. Achieving these results required the design, fabrication and operation of the broad-band electro-optic modulator, the lowjitter SNSPD detector, and the high-resolution TCSPC card. Building upon our demonstration, we believe that the technology exists today to use state-of-the-art ultra-highbandwidth electro-optic modulators, low-jitter single-photon detectors, and commercially available electronics to achieve breakthrough performance sampling in oscilloscope technology. Although conventional oscilloscopes may continue to be the most widely used waveform capture modality for routine usage, and sampling or nonlinear based optical oscilloscopes are useful in certain applications, when the input power is relatively high, this complementary technology may be highly attractive when capturing ultra-high bandwidth optical modulated waveforms at very weak signal levels without directly being subject to conventional limitations.

ACKNOWLEDGMENT

Part of the research, including the W-band modulation, was performed at the Jet Propulsion Laboratory, California Institute of Technology, under contract with the National Aeronautics and Space Administration.

REFERENCES

- Keysight Infiniium UXR-Series (UXR1102A) Oscilloscopes Datasheet.
 Available online at https://www.keysight.com/en/pcx-2935671/uxr-series-real-time-infiniium-oscilloscopes
- [2] LeCroy Labmaster 10zi Datasheet. Available online at http://cdn.teledynelecroy.com/files/pdf/labmaster-10zi-a-datasheet.pdf
- [3] Ultrafast 100 GHz Photodetector XPDV412xR. Finisar Product Specification. Available at https://www.finisar.com/sites/default/files/downloads/xpdv412xr_ultrafast_100_ghz_photodetector_rev_al_product_specification.pdf
- [4] M. Takamiya, M. Mizuno and K. Nakamura, "An on-chip 100 GHz-sampling rate 8-channel sampling oscilloscope with embedded sampling clock generator" Proc. 2002 IEEE International Solid-State Circuits Conference, Paper 11.2 (2002)
- [5] H. Füser, S. Eichstädt, K. Baaske, C. Elster, K. Kuhlmann, R. Judaschke, K. Pierz and M. Bieler "Optoelectronic time-domain characterization of a 100 GHz sampling oscilloscope" Measurement Science and Technology Vol. 23(2), 025201 (2012)
- [6] W. Becker, Advanced Time-Correlated Single Photon Counting Techniques Springer, Berlin (2005). DOI: 10.1007/3-540-28882-1
- [7] V. Shcheslavskiy, P. Morozov, A. Divochiy, Y. Vakhtomin, K. Smirnov, and W. Becker, "Ultrafast time measurements by time-correlated single

- photon counting coupled with superconducting single photon detector," Rev. Sci. Instrum. 87, 053117 (2016).
- [8] A. McCarthy, N. J. Krichel, N. R. Gemmell, X. Ren, M. G. Tanner, S. N. Dorenbos, V. Zwiller, R. H. Hadfield, G. S. Buller, Kilometer-range, high resolution depth imaging via 1560 nm wavelength single-photon detection. Opt. Express 21, 8904–8915 (2013)
- [9] G. Gariepy, N. Krstajić, R. Henderson, C. Li, R. R. Thomson, G. S. Buller, B. Heshmat, R. Raskar, J. Leach and D. Faccio "Single-photon sensitive light-in-fight imaging" Nature Communications, 6, 6021 (2015)
- [10] A. Kirmani, D. Venkatraman, D. Shin, A. Colaço, F. N. C. Wong, J. H. Shapiro, and V. K. Goyal, "First-photon imaging" Science, 343(6166), 58-61 (2014)
- [11] Keysight Infiniium UXR-Series (UXR1102A) Oscilloscopes Datasheet. Available online at https://www.keysight.com/en/pcx-2935671/uxr-series-real-time-infiniium-oscilloscopes
- [12] M. J. Stevens, R. H. Hadfield, R. E. Schwall, S. W. Nam, and R. P. Mirin, "Time-correlated single-photon counting with superconducting singlephoton detectors" Advanced Photon Counting Techniques, ed. Wolfgang Becker, Proc. of SPIE Vol. 6372, 63720U, (2006)
- [13] H. Fedder, S. Oesterwind, M. Wick, I. Shavrin, M. Schlagmuller, F. Olbrich, P. Michler, T. Veigel, M. Berroth, N. Walter, W. Hartmann, W. Pernice, and V. Kovalyuk "Characterization of Electro-Optical Devices with Low Jitter Single Photon Detectors Towards an Optical Sampling Oscilloscope Beyond 100 GHz" Proc. ECOC 2018, Berlin, (2018). Available online at arXiv:1810.05744
- [14] C. Dorrer, C. R. Doerr, I. Kang, R. Ryf, J. Leuthold, P. J. Winzer, "Measurement of eye diagrams and constellation diagrams of optical sources using linear optics and waveguide technology," J. Lightwave Technol. Vol. 23, 178-186 (2005)
- [15] K. Okamoto and F. Ito, "Nearly Shot-Noise-Limited Performance of Dual-Channel Linear Optical Sampling for Ultrafast DPSK Signals" IEEE Journal of Quantum Electronics, Vol. 45(6), 711 (2009)
- [16] W. R. Donaldson, J. R. Marciante, R. G. Roides, "An optical replicator for single-shot measurements at 10 GHz with a dynamic range of 1800:1" IEEE J. Quantum Electron. 46, 191–196 (2010)
- [17] H. Takara, S. Kawanishi, T. Morioka, K. Mori, and M. Saruwatari "100 Gb/s optical waveform measurement with 0.6 ps resolution optical sampling using subpicosecond supercontinuum pulses," Electron. Lett., vol. 30, no. 14, pp. 1153–1153 (1994)
- [18] R. P. Scott, N. K. Fontaine, D. J. Geisler, S. J. B. Yoo, "Frequency-to-Time-Assisted Interferometry for Full-Field Optical Waveform Measurements with Picosecond Resolution and Microsecond Record Lengths", IEEE Photonics Journal, Vol. 4, no. 3, pp. 748-758 (2012)
- [19] J. Li, J. Hansryd, P. O. Hedekvist, P. A. Andrekson, and S. N. Knudsen, "300-Gb/s Eye-Diagram Measurement by Optical Sampling Using Fiber-Based Parametric Amplification" IEEE Photonics Technology Letters, Vol. 13, No. 9, 987-989 (2001)
- [20] S. Lefrancois, Y. Paquot, B. Eggleton, H. Nguyen, D. Wang, S. Set, D. Choi, B. Luther-Davies, and S. Madden, "Terabaud Optical Sampling on a Chalcogenide Optical Chip" Proc. Asia Communications and Photonics Conference, (ACPC), Shanghai, China, paper AF4A (2014). DOI: 10.1364/ACPC.2014.AF4A.3
- [21] M. A. Foster, R. Salem, D. F. Geraghty, A. C. Turner-Foster, M. Lipson and A. Gaeta "Silicon-chip-based ultrafast optical oscilloscope" Nature 456, 07430 (2008)
- [22] P. A. Andrekson, "Picosecond optical sampling using four-wave mixing in fiber," Electron. Lett., vol. 27, no. 16, 1440–1441 (1991)
- [23] B. P. Nelson and N. J. Doran, "Optical sampling oscilloscope using nonlinear fiber loop mirror," Electron. Lett., Vol. 27, 204–205 (1991)
- [24] P. O. Weigel, J. Zhao, K. Fang, H. Al-Rubaye, D. Trotter, D. Hood, J. Mudrick, C. Dallo, A. T. Pomerene, A. L. Starbuck, C. T. DeRose, A. L. Lentine, G. Rebeiz, and S. Mookherjea, "Bonded thin film lithium niobate modulator on a silicon photonics platform exceeding 100 GHz 3-dB electrical modulation bandwidth," Opt. Express 26, 23728-23739 (2018)
- [25] B. A. Korzh, Q-Y. Zhao, S. Frasca, J. P. Allmaras, T. M. Autry, E. A. Bersin, M. Colangelo, G. M. Crouch, A. E. Dane, T. Gerrits, F. Marsili, G. Moody, E. Ramirez, J. D. Rezac, M. J. Stevens, E. E. Wollman, D. Zhu, P. D. Hale, K. L. Silverman, R. P. Mirin, S. W. Nam, M. D. Shaw and K. K. Berggren "Demonstrating sub-3 ps temporal resolution in a superconducting nanowire single-photon detector" arXiv:1804.06839 [physics.ins-det] (2018)
- [26] N. Calandri, Q.-Y. Zhao, D. Zhu, A. Dane, and K. K. Berggren, "Superconducting nanowire detector jitter limited by detector geometry" Appl. Phys. Lett. 109, 152601 (2016)

- [27] F. Marsili, V. B. Verma, J. A. Stern, S. Harrington, A. E. Lita, T. Gerrits, I. Vayshenker, B. Baek, M. D. Shaw, R. P. Mirin, and S. W. Nam, "Detecting single infrared photons with 93% system efficiency" Nature Photonics 7, 210 (2013).
- [28] X. Wang, B. A. Korzh, P. O. Weigel, D. J. Nemchick, B. J. Drouin, A. Fung, W. Becker, Q. Zhao, D. Zhu, M. Colangelo, A. E. Dane, K. K. Berggren, M. D. Shaw, and S. Mookherjea, "Oscilloscopic capture of 100 GHz modulated optical waveforms at femtowatt power levels," in Optical Fiber Communication Conference Postdeadline Papers 2019, (Optical Society of America, 2019), paper Th4C.1.
- [29] K. J. Quirk, J. W. Gin and M. Srinivasan, "Optical PPM synchronization for photon counting receivers," MILCOM 2008 - 2008 IEEE Military Communications Conference, San Diego, CA, pp. 1-7, (2008)
- [30] C. M. J. Wang, P. D. Hale, J. A. Jargon, D. F. Williams and K. A. Remley, "Sequential Estimation of Timebase Corrections for an Arbitrarily Long Waveform," in IEEE Transactions on Instrumentation and Measurement, vol. 61, no. 10, pp. 2689-2694, (2012)
- [31] Jaspreet Sahota and Daniel F. V. James, "Quantum-enhanced phase estimation with an amplified Bell state," Phys. Rev. A, 88, 063820, (2013)
- [32] J. Arlt, D. Tyndall, B. R. Rae, D. D.-U. Li, J. A. Richardson, and R. K. Henderson, "A study of pile-up in integrated time-correlated single photon counting systems" Review of Scientific Instruments 84, 103105 (2013)
- [33] Y. Wang, J. Kuang, C. Liu, and Q. Cao " A 3.9-ps RMS Precision Time-to-Digital Converter Using Ones-Counter Encoding Scheme in a Kintex-7 FPGA" IEEE Transactions on Nuclear Science, vol. 64, no. 10, pp. 2713-2718, (2017).

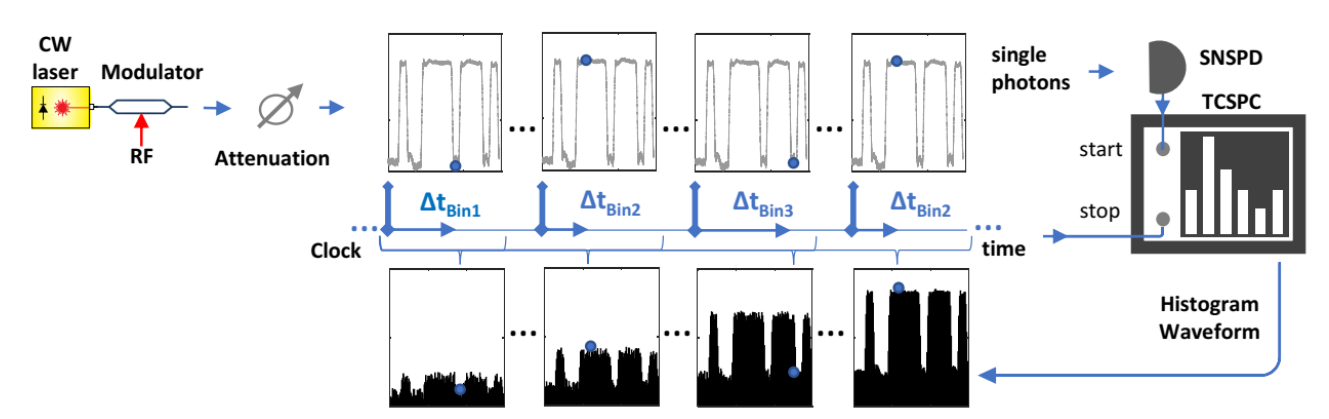


Fig. 1. Experimental setup and working principle. The optical power after the modulator was heavily attenuated so that the detector detected, on average, less than one photon per clocking window. Detected single photons started the time interval recorded on the TCSPC card until the next trigger pulse from the "Clock" stopped the time interval. The time interval was saved into a list of start-stop time lengths, time-tagging each photon detection event. This list of time-tags was used to build a histogram, which directly reconstructs the modulated waveform.

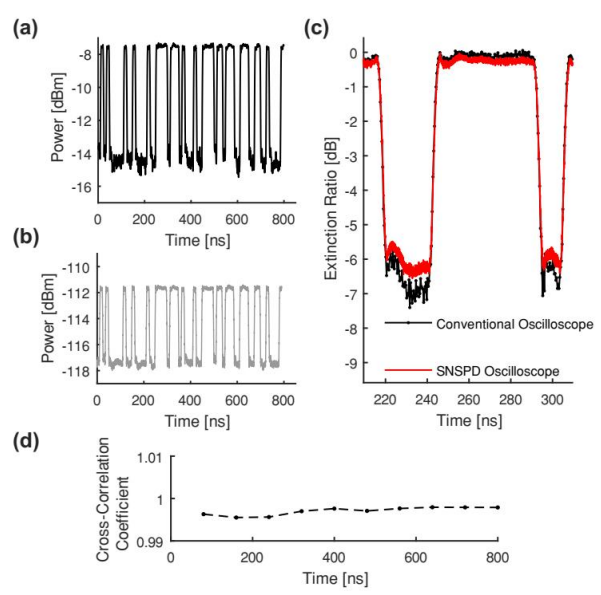


Fig. 2. (a) Bit sequence detected by a 20 GHz photodiode (optical module in a conventional sampling oscilloscope) at -7 dBm received power. (b) Same bit sequence detected by the single photon TCSPC oscilloscope method after 105 dB additional attenuation. (c) Overlay of the same bit sequence under the two different methods showing high fidelity. (d) Quantitative comparison showing accuracy of replicas.

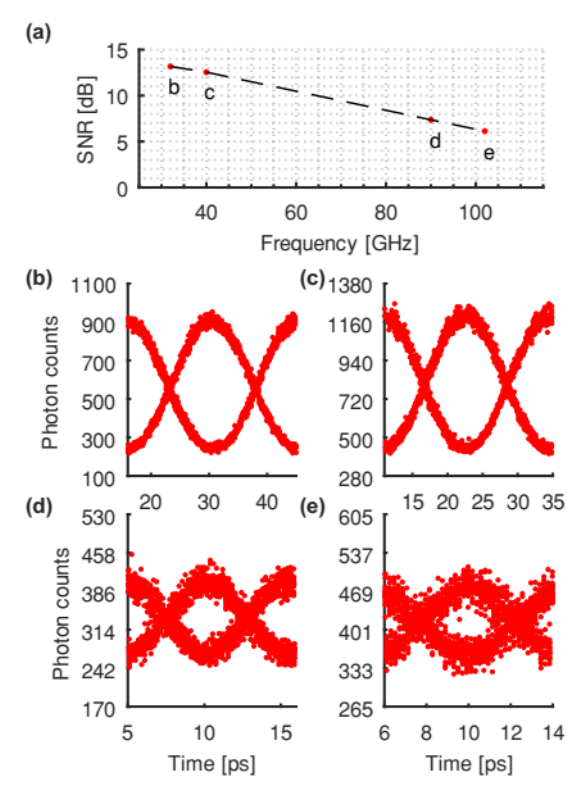


Fig. 3. (a) Signal to noise ratio (SNR) calculated from the acquired data, captured at an input average optical power of 64 fW and an acquisition time of 120 s in each case, versus various modulation frequencies from 32 GHz to 102 GHz. (b)-(e) Eye diagrams were constructed from the waveforms, with a calculated SNR of 13.2 dB at 32 GHz, 12.5 dB at 40 GHz, 7.36 dB at 90 GHz, 6.13 dB at 102 GHz.

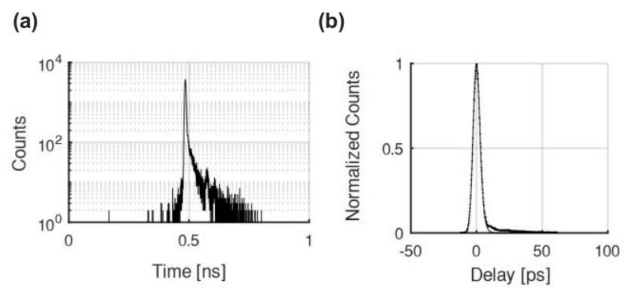


Fig. 4. (a) The instrument response function (IRF) for the data reported in Fig. 4 was measured using a mode-locked fiber laser at 1550 nm wavelength, with a nominal output optical pulse width of 0.5 ps. (b) The raw data, with the mean-value (in time) subtracted out, was fit to an exponentially modified Gaussian function. The fitted value of the full width at half-maximum (FWHM) is 6.32 ps.

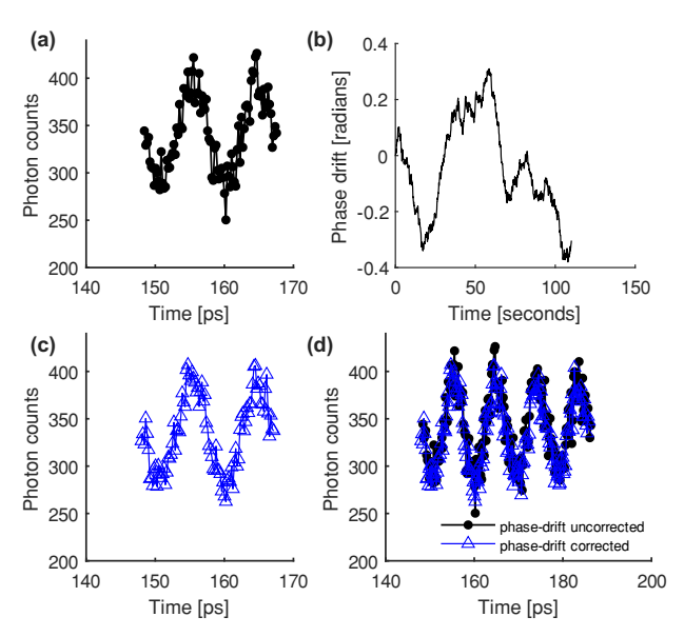


Fig. 5. (a) Raw waveform prior to phase drift correction. (b) The drift between the trigger and the signal was dominated by a slow variation of the phase over the span of the collection time, with 0.19 radians root-mean-squared (r.m.s.) amplitude. The drift was extracted by sliding a 10 second window by 0.1 second increments over the time-tagged dataset and creating a histogram of the counts in each window, which was then fit to a vertically shifted sinusoid function. The window was large enough so that a fit could be extracted giving a phase estimate with a 95% confidence interval and standard error smaller than the maximum slope of the phase change per time-step. The phase drift of the 102 GHz signal is shown here. (c) Segment of phase drift corrected waveform. (d) Overlaid waveforms.

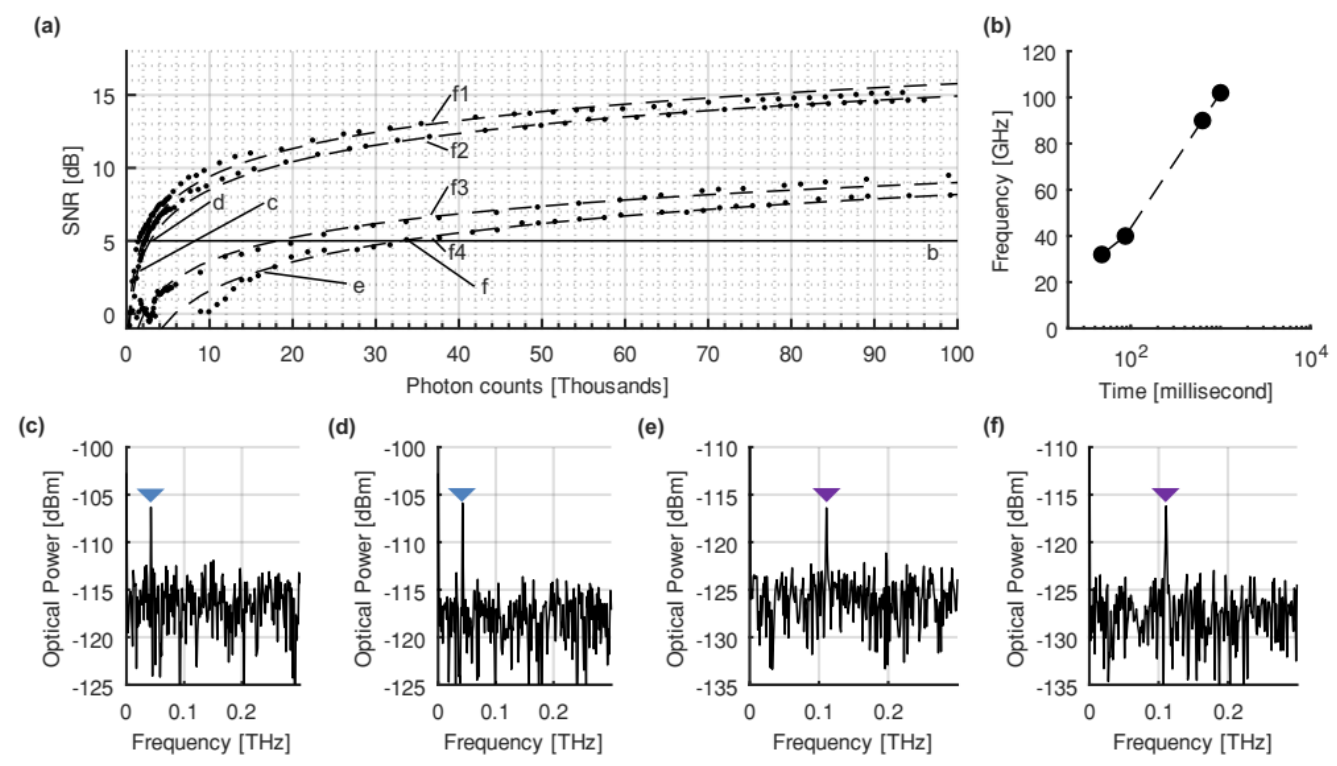


Fig. 6. (a) The SNR of the frequency-domain peak, identifying the frequency of the sinusoidal wave from the calculated Fourier transform of the measured data, was calculated from snapshots of the data acquired as the measurement gradually progressed. Markers f1 through f4 represent modulation frequencies 32 GHz, 40 GHz, 90 GHz, and 102 GHz, respectively. Markers c through f refer to Fig.6 (c)-(f). (b) Acquisition time to reach SNR = 5, an arbitrarily chosen representative value, versus the modulation frequency. (c)-(d) Calculated power spectral densities for 40 GHz modulation at (c) SNR=3, and (d) SNR = 5, showing that the signal peak has been detected and remains the same, whereas the noise floor decreases. (e)-(f) Calculated power spectral densities for 102 GHz modulation at (e) SNR=3, and (f) SNR = 5, showing a similar behavior.